高等学校化学学报
CHEMICAL JOURNAL OF CHINESE UNIVERSITIES
研究论文

基于动态氢键网络协同调控AIE与力学性能的多响应水凝胶

张阳戴翼，邵　研，姜世梅
（吉林大学化学学院，超分子结构与材料全国重点实验室，长春130012）

摘要　通过将聚集诱导发光(AIE)分子NE共价整合到由咪唑和羧酸基团组成的动态氢键网络中，构建了一种多刺激响应荧光水凝胶P(VI-*co*-MAAC-NE). 致密的氢键网络不仅增强了材料的机械强度，还通过限制NE分子运动显著提升了其AIE效应. 在各种外部刺激下，氢键发生可逆的解离和重构，从而协同调控水凝胶的力学性能和AIE发光行为：有机溶剂破坏氢键和NE聚集，导致凝胶溶胀并猝灭荧光. 在强酸性条件下，NE分子的质子化抑制了分子内电荷转移(ICT)过程，产生蓝移发射并呈现强烈蓝色荧光. 在高碱性环境中，羧基的去质子化会引起溶胀并分散NE聚集体，从而显著猝灭荧光. 此外，该体系表现出热激活形状记忆特性，加热到玻璃化转变温度(T_g≈62 ℃)以上可使水凝胶软化以实现可编程重塑，随后在常温下氢键重构可固定形状且不损害荧光性能. 这些多重刺激响应与形状记忆特性展示了P(VI-*co*-MAAC-NE)水凝胶在信息加密与防伪领域的应用潜力. 该工作为传感与信息存储提供了实用的材料平台，同时为融合AIE特性与动态网络结构的智能软材料设计提供了新思路.

关键词　聚集诱导发光(AIE)；多响应水凝胶；机械性能；氢键网络
中图分类号　O632　　**文献标志码**　A　　doi：10.7503/cjcu20250381

Multi-responsive Hydrogel Featuring Synergistic Regulation of AIE and Mechanical Behaviors *via* Dynamic Hydrogen Bonding Network

ZHANG Yangdaiyi, SHAO Yan, JIANG Shimei*
(*State Key Laboratory of SupramolecularStructure and Materials*, *College of Chemistry*, *Jilin University*, *Changchun* 130012, *China*)

Abstract　A multi-stimuli-responsive hydrogel, P(VI-*co*-MAAC-NE), was successfully constructed by covalently integrating the aggregation-induced emission(AIE) moiety(*Z*)-N-(4-(1-cyano-2-(4-(diethylamino)phenyl)vinyl)-phenyl) methacrylamide (NE) into a dynamic hydrogen-bonding network composed of 1-vinylimidazole (VI) and methacrylic acid (MAAC) groups. The dense hydrogen-bonding network not only provides enhanced mechanical robustness, but also significantly enhances the AIE effect of NE by restricting its molecular motion. Under various external stimuli, the hydrogen bonds within the hydrogel network undergo reversible dissociation and reformation, thus enabling synergistic modulation of the hydrogel's mechanical properties and luminescence behavior. Specifically, organic solvents disrupt the hydrogen-bonding network and the aggregation of the AIE moiety NE, resulting in macroscopic swelling and fluorescence quenching of the hydrogel. In strongly acidic conditions, protonation of NE molecules suppresses the intramolecular charge transfer (ICT) process, yielding a blue-shifted emission band accompanied by intense blue fluorescence; in highly alkaline environments, deprotonation of carboxyl groups induces hydrogel swelling and disperses NE aggregates, leading to pronounced fluorescence quenching.

收稿日期：2025-12-16. 网络首发日期：2026-03-09.
联系人简介：姜世梅，女，博士，教授，主要从事智能响应超分子材料方面的研究. E-mail：smjiang@jlu.edu.cn
基金项目：国家自然科学基金(批准号：52173167)资助.
Supported by the National Natural Science Foundation of China(No.52173167).

Moreover, the system exhibits thermally activated shape-memory behavior: heating above the glass transition temperature (T_g: *ca.* 62 ℃) softens the hydrogel to allow programmable reshaping, and subsequent hydrogen bond reformation at ambient conditions locks in the resultant geometries without sacrificing the hydrogel's fluorescence performance. By capitalizing on these multi-stimuli-responsive characteristics and shape-memory behavior, the potential of hydrogel P(VI-*co*-MAAC-NE) for advanced information encryption and anti-counterfeiting applications is demonstrated. This work not only provides a versatile material platform for sensing and information storage, but also offers new insights into the design of intelligent soft materials integrating AIE features with dynamically regulated supramolecular network structures.

Keywords Aggregation-induced emission (AIE); Multi-responsive hydrogel; Mechanical properties; Hydrogen bonds network

1 Introduction

Fluorescent hydrogels have attracted considerable interest for applications in sensing[1—3], bioimaging[4—6], bionic actuation[7,8], and information encoding[9—11], owing to their soft porous structure, tunable luminescence, and dynamic exchange of substances with the surrounding environment[12,13]. To date, various luminescent species such as fluorescent proteins[14], conventional organic dyes[15,16], and carbon dots[17,18] have been incorporated into hydrogel matrices to construct stimulus-responsive intelligent systems. However, these systems often suffer from intrinsic limitations: hydrophobic planar dyes tend to undergo dense π-π stacking within hydrophilic polymer networks, leading to aggregation-caused quenching (ACQ) and severe emission quenching at high concentrations, which significantly restricts their practical applicability[19,20].

The concept of aggregation-induced emission (AIE), proposed by Tang Benzhong *et al.* in 2001, has opened up new avenues for the design of organic luminescent materials that exhibit intense emission in the aggregated state[21]. In contrast to traditional ACQ dyes, AIE molecules in a well-dispersed state show weak emission because intramolecular rotational motion dissipates excitation energy. However, upon aggregation, restricted molecular motion and twisted conformations effectively suppress detrimental π-π stacking interactions, thus enabling bright fluorescence emission[22—25]. Most AIEgens are hydrophobic and therefore tend to emit intensely in aqueous or hydrophilic environments. Fortunately, hydrogels (highly hydrated three-dimensional networks) serve as ideal matrices to promote the aggregation of AIEgens, thereby facilitating strong and stable fluorescence emission[26,27].

Despite such inherent compatibility, the integration of AIEgens into hydrogel matrices remains a formidable challenge. Physical blending often leads to macroscopic phase separation between hydrophobic AIEgens and the hydrophilic polymer network, giving rise to heterogeneous fluorescence emission[28]. In addition, copolymerizing AIEgens into the hydrogel backbone tends to compromise the resultant material's mechanical strength; conversely, an insufficient loading of AIEgens fails to drive effective molecular aggregation, thus yielding faint fluorescence output. Therefore, the fabrication of AIE-active hydrogels simultaneously endowed with superior mechanical strength, intense fluorescence, and homogeneous emission still constitutes a major bottleneck[29,30]. Moreover, in most reported systems, AIEgens and hydrogel network respond independently to external stimuli, leading to non-synergistic optical and mechanical behaviors that severely restrict real-time sensing and feedback capabilities[31—33].

To address these challenges, we constructed a multi-stimuli-responsive fluorescent hydrogel, P(VI-*co*-MAAC-NE), *via* the copolymerization of the aggregation-induced emission(AIE) monomer(*Z*)-N-(4-(1-cyano-2-(4-(diethylamino)phenyl)vinyl)-phenyl)methacrylamide (NE) into a dynamic hydrogen-bonding network composed of 1-vinylimidazole (VI) and methacrylic acid (MAAC) units. The NE monomer possesses a

cyanostilbene backbone that endows it with AIE characteristics, alongside terminal *N*,*N*-diethylaniline groups responsible for its stimuli-responsive behavior. The VI and MAAC units form robust yet dynamic hydrogen bonds, which not only enhance the hydrogel's mechanical performance, but also restrict the intramolecular motion of NE, thereby boosting its fluorescence emission. Crucially, these hydrogen bonds exhibit reversible responsiveness to multiple external stimuli, enabling orthogonal modulation of the hydrogel's fluorescent and mechanical properties. For instance, organic solvents[*e.g.*, dimethyl sulfoxide(DMSO)] disrupt the hydrogen-bonding network and NE aggregation, resulting in fluorescence quenching, hydrogel swelling, and mechanical softening. Under acidic conditions, both VI and NE undergo protonation: this breaks hydrogen bonds and terminates the intramolecular charge transfer(ICT) process in NE, leading to a 39 nm blue-shift and intense blue fluorescence. In alkaline environments, carboxylate deprotonation induces hydrogel swelling and disperses NE aggregates, achieving 99.5% fluorescence quenching. Heating above the glass transition temperature (T_g) also disrupts hydrogen bonds, enabling programmable shape deformation; subsequent cooling restores the network structure and permanently fixes the deformed shape. Leveraging these integrated multi-stimuli-responsive and shape-memory properties, we further demonstrate the great potential of this hydrogel for fluorescent information storage and encryption applications.

2 Experimental

2.1 Materials and Measurements

All the solvents were purchased from commercial suppliers and used directly without further purification unless otherwise stated. 1-Vinylimidazole(VI), methacrylic acid(MAAC), *N*,*N*′-methylenebisacrylamide(Bis, 99%), azobisisobutyronitrile(AIBN, 98%), and potassium persulfate(KPS) were all purchased from Energy Chemical Co., Ltd.

UV-Vis absorption spectra were recorded on a Shimadzu 3600 UV-Vis spectrometer. Fluorescence spectra were measured on a Shimadzu RF-5301PC fluorescence spectrophotometer with an excitation wavelength of 365 nm. Fourier-transform infrared(FTIR) spectra were recorded on a Bruker VERTEX 70 FTIR spectrometer. Scanning electron microscopy(SEM) images were obtained from a JEOL JEM-6700F scanning electron microscope with 3 kV operating voltage. Differential scanning calorimetry(DSC) was performed on a DSC Q20 instrument under a nitrogen purge. Rheological measurements were carried out on a TA HR-2 rheometer with parallel plate geometry. The mechanical property tests were carried out using a universal testing machine(ITW 5944 2KN).

2.2 Synthesis of NE

The synthesis and characterization of NE has been reported in our previous work[8].

2.3 Preparation of P(VI-*co*-MAAC-NE) Hydrogel

NE(20 mg, 0.05 mmol), VI(370 μL, 4.10 mmol), MAAC(1.985 mL, 23.40 mmol), Bis(42.40 mg, 0.27 mmol), and AIBN(23 mg, 0.15 mmol) were dissolved in 7.65 mL DMSO. The precursor solution was injected into a mold(composed of a 1 mm rubber spacer sandwiched between glass plates) and thermally polymerized at 70 ℃ for 8 h to yield a yellow transparent organogel. Subsequently, the organogel was immersed in water for solvent exchange(with water replaced 3—4 times daily over 7 d) to remove residual DMSO, ultimately producing a green fluorescent hydrogel. By varying the NE content(1—30 mg), hydrogels with tunable fluorescence emission were successfully fabricated.

2.4 Preparation of P(VI-*co*-MAAC) Hydrogel

P(VI-*co*-MAAC) hydrogel was prepared following the procedure for P(VI-*co*-MAAC-NE) hydrogel, excluding NE.

2.5 Preparation of PVI Hydrogel

VI(2.72 mL, 30 mmol), Bis(42.40 mg, 0.27 mmol), and AIBN(23 mg, 0.15 mmol) were dissolved in toluene(7.29 mL). The mixture was polymerized in an oven at 70 ℃ for 8 h to yield the PVI hydrogel.

2.6 Preparation of PMAAC Hydrogel

MAAC(2.55 mL, 30 mmol), Bis(42.40 mg, 0.27 mmol), and initiator potassium persulfate(KPS, 27.20 mg, 0.10 mmol) were thoroughly mixed in deionized water(7.46 mL). The homogeneous solution was polymerized in an oven at 70 ℃ for 8 h to obtain the PMAAC hydrogel.

2.7 Mechanical Measurement

Samples were cut into strips(30 mm×5 mm×1 mm) and clamped onto a universal testing machine. Tensile tests were performed at a compression speed of 100 mm/min with a 100 N load cell.

For solvent-responsiveness characterization, the hydrogel samples were first fully swollen in deionized water until reaching equilibrium. The equilibrated samples were then immersed in DMSO until equilibrium was reached(usually 48 h). After gently removing the surface liquid with filter paper, the DMSO-swollen gel was subjected to tensile measurement. To evaluate reversibility, the same batch of samples was subsequently dialyzed back to deionized water to restore the hydrogel state, and measurements were taken again.

For pH responsiveness, the hydrogel samples were immersed in aqueous solutions with different pH values(adjusted using 1 mol/L HCl or 1 mol/L NaOH) until swelling equilibrium was reached(typically 48 h). The pH value of the surrounding solution was verified using a calibrated pH meter. Before conducting mechanical measurement, the surface of the pH-treated hydrogel strips was gently blotted dry. Tensile measurement were performed on samples equilibrated under each specific pH condition.

For temperature-dependent measurement, a water bath attachment was integrated into the testing system. Samples were equilibrated in water at temperatures ranging from 10 ℃ to 70 ℃ prior to measurement.

2.8 Micro Morphology Characterization

Hydrogels were cut into blocks, freeze-dried, and the microscopic morphology of the cross-section was observed. Due to the poor conductivity of the polymer matrix, gold spraying treatment was used before characterization to enhance surface conductivity. Then, SEM was performed on the gel samples by using a JEOL JEM-6700F emission scanning electron microscope, with the accelerating voltage of 3 kV.

2.9 Swelling Ratio Measurement

Identically shaped hydrogel specimens were softly wiped with filter paper to remove surface water and weighed(m_0, g). Later, gels were soaked into aqueous solutions of varying pH value(equilibrated for 24 h). Swollen gels were re-weighed(m_t, g) following surface water removal. Triplicate measurements were averaged, and the swelling ratio(η, %) was calculated as follows[34].

$$\eta = \frac{m_0 - m_t}{m_0} \times 100\%$$

2.10 Glass Transition Temperature Measurement

In Rheological measurement, cylindrical hydrogel specimens(25 mm diameter×50 mm height) were prepared and coated with silicone oil to minimize solvent evaporation. The samples were loaded onto a rheometer equipped with 25 mm parallel plates. Temperature sweeps were conducted from 30 ℃ to 90 ℃ at a heating rate of 5 ℃/min under oscillatory shear conditions(frequency: 1 Hz; strain amplitude: 0.05%). T_g was identified as the peak value of the loss factor(tanδ) curve. In differential scanning calorimetry(DSC) analysis, approximately 10 mg of hydrogel was hermetically sealed in an aluminum crucible. DSC scans were performed from 30 ℃ to 75 ℃ at a heating rate of 5 ℃/min. The T_g was determined using the midpoint method, where the intersection of the extrapolated baselines(pre- and post-transition) with the DSC curve's inflection region corresponds to the glass transition temperature.

2.11 UV-Vis and Fluorescent Spectral Measurement of NE

NE was dissolved in DMSO at a concentration of 10^{-3} mol/L. Subsequently, it was diluted with aqueous solutions containing varying amounts of HCl and NaOH to obtain a mixed solution with a water content of 90% and a final NE concentration of 10^{-4} mol/L. Spectral analysis was then performed.

3 Results and Discussion

3.1 Preparation of P(VI-*co*-MAAC-NE) Hydrogel

P(VI-*co*-MAAC-NE) organogel was first prepared through radical copolymerization of NE, VI, and MAAC in DMSO, using AIBN as the initiator and Bis as the crosslinker (Scheme 1). This organogel displayed relatively weak mechanical strength and low fluorescence emission, showing a Young's modulus(E) of 55.80 kPa, breaking strain(ε_b) of 138.47%, and tensile breaking stress(σ_b) of 77.27 kPa[Fig.1(A)]. Subsequently, the organogel was transformed into the target hydrogel, P(VI-*co*-MAAC-NE), *via* solvent exchange with water to remove residual DMSO. This transition led to a remarkable enhancement in both mechanical and fluorescence properties. Tensile tests revealed typical yielding behavior at low strain, followed by plastic deformation, strain hardening, and necking at higher strains. The mechanical parameters increased significantly, with E, ε_b, and σ_b reaching 166.67 MPa, 132.26%, and 2.79 MPa, respectively [Fig.1(A)]. Meanwhile, the hydrogel showed intense green fluorescence centered at 504 nm, with an emission intensity approximately 105 times higher than that of the organogel[Fig.1(B)].

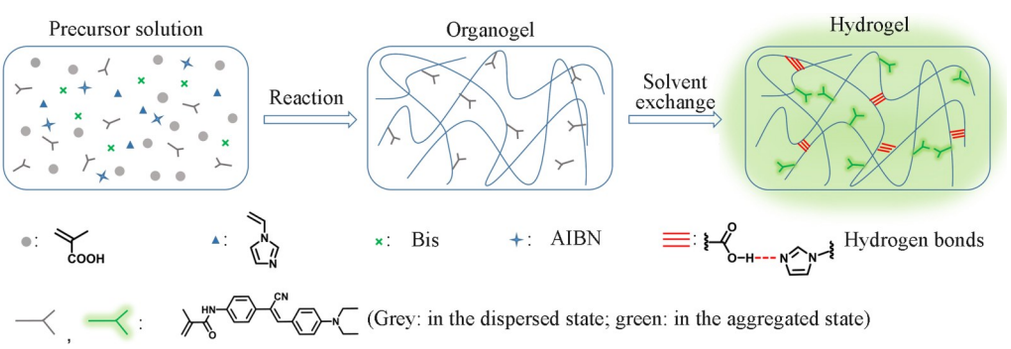

Scheme 1 Schematic diagram of the preparation of P(VI-*co*-MAAC-NE) hydrogel

The remarkable concurrent in mechanical strength and fluorescence was attributed to the formation of a dense hydrogen-bonding network between the imidazole and carboxylic acid groups[35]. The FTIR analysis results showed that in P(VI-*co*-MAAC) and P(VI-*co*-MAAC-NE) hydrogels, the C═N stretching vibration of PVI shifted from 1500 cm^{-1} to 1545 cm^{-1}, while the C═O stretching vibration of PMAAC shifted from 1706 cm^{-1} to 1710 cm^{-1}, which confirmed the strong intermolecular interactions[Fig.1(C) and (D)]. The overall spectral profile of P(VI-*co*-MAAC-NE) closely resembled that of PMAAC, consistent with the dominant content of methacrylic acid in the copolymer. No distinct cyano stretching peak was observed, likely due to the low incorporation level of NE. Beyond the primary hydrogen bonds between imidazole and carboxylic acid groups, additional cohesion of the network arose from hydrogen bonding among carboxylic acid groups themselves and hydrophobic interactions between imidazole moieties in the aqueous environment, all of which synergistically enhanced the overall mechanical properties[36]. The resulting shortened interchain distances promoted the formation of a densely porous network morphology, as observed by SEM(Fig.S1, see the Supporting Information of this paper), which further accounted for the improved mechanical performance.

This hydrogen-bonding network also played a crucial role in fluorescence enhancement by effectively restricting the molecular motion of the incorporated NE. The NE exhibited typical AIE behavior, attributable to its twisted cyanostilbene backbone. In dispersed states, the free rotation of benzene rings in the

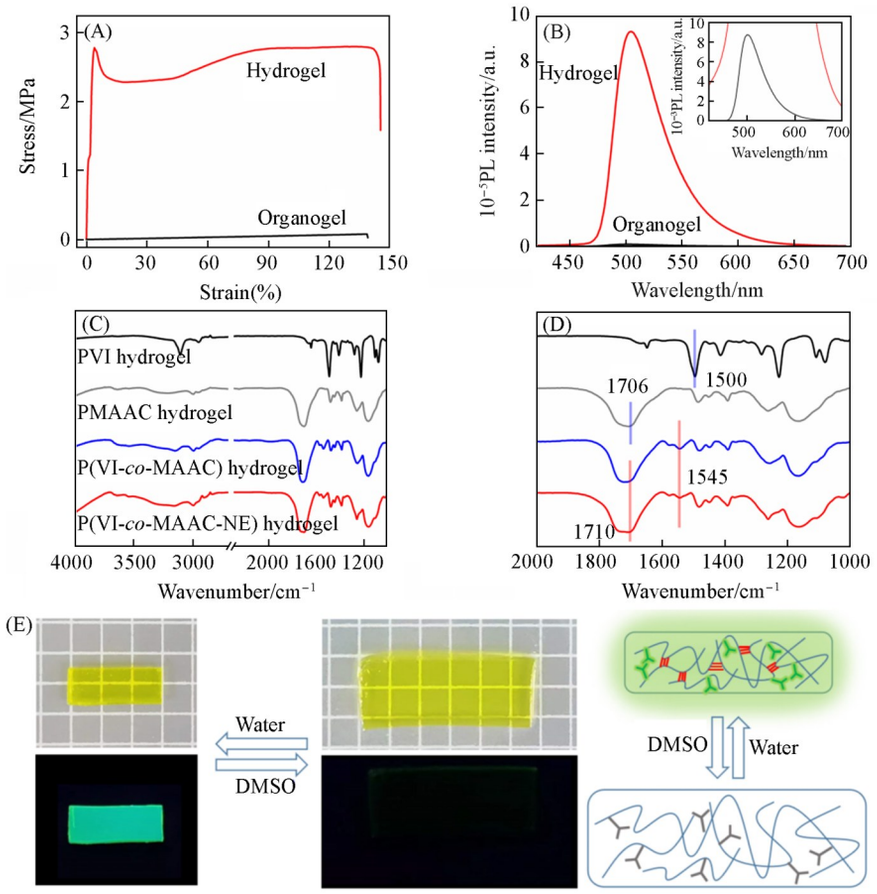

Fig. 1 Stress-strain curves(A) and fluorescence spectra(B) of hydrogel and organogel, FTIR spectra(C, D) of PVI hydrogel, PMAAC hydrogel, P(VI-*co*-MAAC) hydrogel and P(VI-*co*-MAAC-NE) hydrogel, photographs of swelling behavior and fluorescence change(E) of P(VI-*co*-MAAC-NE) hydrogel in DMSO and water under natural light and UV light after reaching equilibrium, along with a schematic illustration of the internal structural change(the length of each grid is 0. 5 cm)

cyanostilbene unit dissipated absorbed energy *via* non-radiative pathways, resulting in weak fluorescence. In contrast, in aggregated states, molecular rotation was restricted[8]. When copolymerized into the hydrogel network, the motion of NE molecules was effectively constrained by the strong hydrogen bonds between polymer chains, promoting radiative transition and leading to intense emission. By varying the amount of NE incorporated, a series of highly fluorescent hydrogels was obtained. As the NE content increased, the emission peak exhibited a gradual red-shift(Fig.S2, see the Supporting Information of this paper), attributed to the formation of J-aggregates[37]. For further investigation, we selected the hydrogel containing 20 mg of NE, which showed an emission maximum at 504 nm, indicating a high degree of NE aggregation suitable for subsequent modulation.

3.2 Solvent Responsiveness

As established above, the mechanical and fluorescent properties of P(VI-*co*-MAAC-NE) hydrogel were governed by its internal hydrogen-bonding network. Therefore, any stimulus capable of altering the hydrogen bonds could effectively modulate its properties. To verify this, we employed organic solvent to disrupt and subsequently restore the hydrogen bonds. Upon immersion in DMSO until equilibrium swelling, the hydrogel exhibited significant volumetric expansion, a pronounced decrease in mechanical strength, and substantial fluorescence quenching[Fig. 1(E)]. This behavior was attributed to the dissociation of hydrogen bonds by

DMSO, which loosened the polymer network and allowed solvent penetration[35,38]. Concurrently, the disruption of hydrogen bonds reduced NE aggregation, and DMSO, acting as a good solvent for NE, enhanced molecular mobility, thereby suppressing the AIE effect. Importantly, when the gel was dialyzed back into water, its fluorescence, volume, and mechanical properties were fully recovered[Fig.1(A) and (B)]. This cycle could be repeated at least 3 times, confirming the highly reversible nature of the solvent-triggered destruction and reformation of hydrogen bonds(Fig.S3, see the Supporting Information of this paper).

3.3 pH Responsiveness

In addition to solvent, pH stimulation served as another effective approach for tuning the mechanical and fluorescence properties of P(VI-*co*-MAAC-NE) through reversible disruption of hydrogen bonds. A series of hydrogel samples was immersed in aqueous solutions of different pH values until swelling equilibrium. Their volumetric swelling, mechanical properties, and fluorescence were measured and correlated.

Within the pH range of 2—10, the volume, mechanical properties and fluorescence remained largely unchanged, indicating the stability of the hydrogen-bonding network under these conditions, and the hydrogel preserved AIE behavior[Fig.2(A)].

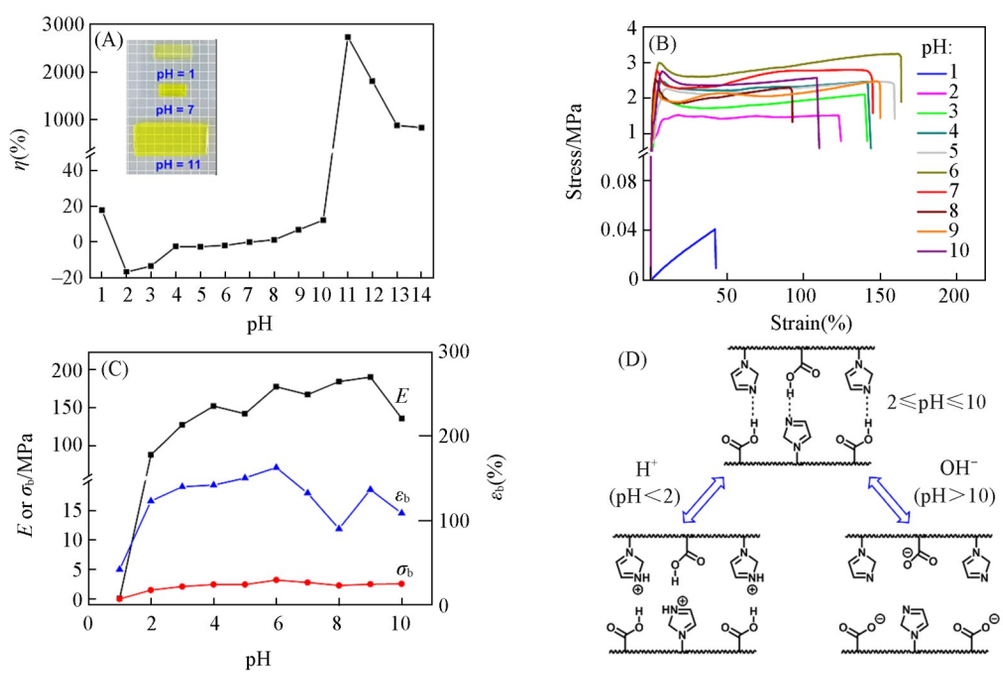

Fig. 2 Swelling ratio(A), stress-strain curves(B) and corresponding Young's modulus(E), breaking strain (ε_b), and tensile breaking stress(σ_b)(C) of P(VI-*co*-MAAC-NE) hydrogel at different pH values, and schematic illustration of hydrogen-bonding changes in P(VI-*co*-MAAC-NE) hydrogel under different pH conditions(D)

However, under strong acidic conditions(pH=1), the hydrogel exhibited a coupled response. Marked swelling occurred, with the swelling ratio increasing by approximately 20% compared to the initial state [Fig.2(A)]. Correspondingly, the mechanical parameters decreased significantly: E, ε_b, and σ_b dropped to 0.12 MPa, 41.99%, and 0.04 MPa, respectively. The tensile curve no longer exhibited yielding behavior, indicating a transition to a fully elastic gel state[Fig.2(B) and (C)]. This transformation was attributed to the protonation of imidazole groups under strong acidity, which disrupted the hydrogen bonds between imidazole and carboxylic acid units[39]. The resulting electrostatic screening further weakened the polymer network, leading to volumetric expansion[Fig.2(D)].

At the same time, a pronounced fluorescence change was observed: intense blue emission centered at

465 nm[Fig.3(A)]. This emission shift was intrinsically linked to the protonation of the fluorophore NE. NE featured a cyanostilbene backbone with terminal *N*,*N*-diethylaniline groups, where the twisted conformation endowed it with distinct AIE characteristics. Moreover, the cyanostilbene unit functioned as an electron acceptor(A), connected *via* a π-conjugated benzene bridge to the electron donating *N*,*N*-diethylaniline group (D), forming a typical D-π-A structure that supported an ICT process[8]. Building on the established ICT characteristics of NE, we further investigated how external stimuli could modulate its photophysical properties through structural alterations. Disturbances to the D-π-A structure were expected to disrupt the ICT process, leading to significant changes in emission color and intensity[40,41]. In the case of NE, protonation of the *N*,*N*-diethylaniline group under acidic conditions played a key role.

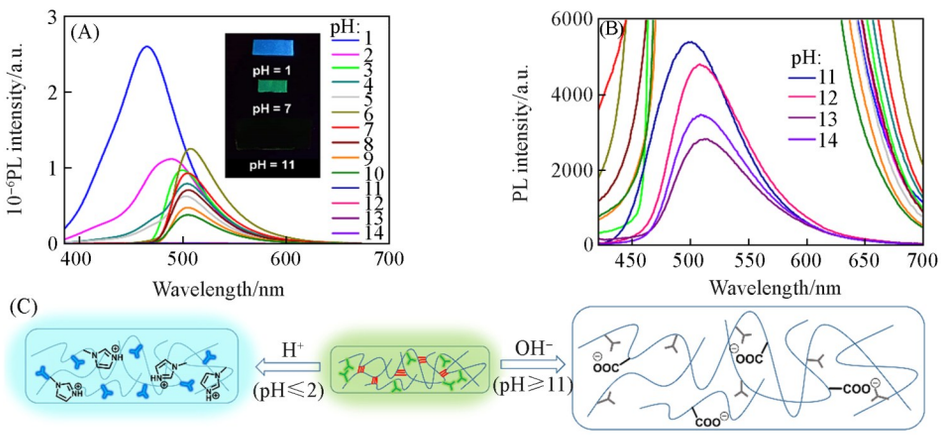

Fig. 3 Fluorescence spectra(A, B) of P(VI-*co*-MAAC-NE) hydrogel measured under different pH conditions, and schematic illustration of the structural changes(C) of the hydrogel in strongly acidic(pH≤2) and strongly alkaline(pH≥11) environments

To simulate the acidic response of NE within hydrogel environment, aggregated states of NE were prepared in 90% aqueous mixtures at varying pH levels. Under neutral and alkaline conditions, green emission was observed near 515 nm. In acidic media, however, the absorption peak blue-shifted to 330 nm, and the emission peak shifted to 466 nm, accompanied by a nearly 30-fold enhancement in intensity (Fig. S4, see the Supporting Information of this paper). This dramatic transition was attributed to the protonation of the electron donating diethylaniline group, which converted into an electron accepting moiety. The resultant disruption of the D-π-A structure suppressed the ICT effect, shifting absorption to the UV region and turning the weak green emission into intense blue fluorescence. Thus, under strong acid, a single stimulus triggers two parallel effects: network disruption (governing mechanics/volume) and fluorophore protonation(governing emission), resulting in a coupled multi-parameter response.

In contrast, under strongly alkaline conditions (pH>11), deprotonation of carboxylic acid groups (—COOH) to carboxylate ions(—COO^-) broke the hydrogen bonds and formed strong electrostatic repulsion among polymer chains. This caused rapid swelling and made the hydrogel too fragile for mechanical testing. As the pH increased beyond 11, a slight contraction in gel volume was observed compared to that at pH=11 [Fig.2(A)], which was ascribed to the elevated ionic strength in the environment that partially shielded the interchain electrostatic repulsion. In terms of fluorescence, although the emission remained in the green region (near 504 nm), the intensity dropped by approximately 186-fold[Fig.3(B)]. This severe quenching was a direct result of the hydrogel's extreme swelling[Fig.3(C)], which dispersed the NE aggregates and reactivated non-radiative decay pathways[42,43]. Therefore, under strong alkaline conditions, the dissociation of hydrogen-bonding network acted as a common cause, synergistically driving both the macroscopic swelling/mechanical failure and the microscopic dispersion of AIEgens that leaded to fluorescence quenching.

The correlation between the swelling ratio, Young's modulus, and fluorescence intensity at different pH values is summarized in Fig. S5 (see the Supporting Information of this paper). This quantitative analysis provides a clear visual demonstration of the synergistic coupling observed under strongly alkaline conditions and the distinct dual-pathway response occurring under highly acidic conditions. To evaluate the reversibility of the pH-responsive behavior, the hydrogel was repeatedly subjected to multiple cycles of alternating immersion in pH=1 and pH=11 solutions, with equilibration in deionized water (pH=7) in between. After completing each cycle, both the fluorescence intensity and mechanical properties returned to their initial values, demonstrating excellent reversibility (Fig.S6, see the Supporting Information of this paper).

3.4 Temperature Responsiveness

The hydrogen-bonding network in P(VI-*co*-MAAC-NE) also exhibited distinct temperature response behavior. As the temperature increased from 10 ℃ to 70 ℃, the hydrogel became progressively softer and more stretchable. Its E and σ_b decreased from 173.17 and 3.14 MPa to 25.84 and 1.02 MPa, respectively, while the ε_b increased from 129.52% to 322.04%. The yielding behavior gradually diminished over this range, indicating a transition from plastic deformation at low temperatures to elastic deformation at elevated temperatures [Fig.4(A) and (B)][44,45].

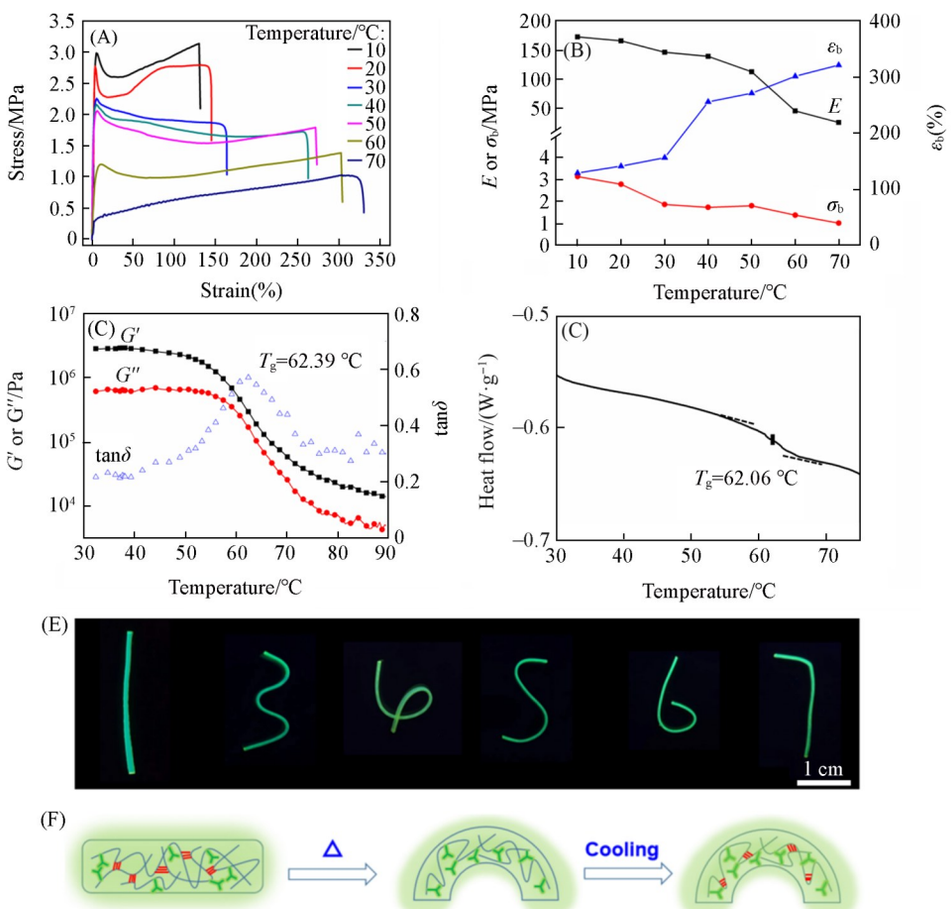

Fig. 4 Stress-strain curves(A) and corresponding E, ε_b, and σ_b(B) of the hydrogel measured at different temperatures(tensile rate: 100 mm/min), temperature-sweep rheological curve from 30 ℃ to 90 ℃ (frequency: 1 Hz, strain: 0.05%)(C), DSC thermogram obtained at a heating rate of 5 ℃/min(D), shape-memory behavior of a strip-shaped P(VI-*co*-MAAC-NE) hydrogel observed under UV light (the scale bar is 1 cm)(E), and schematic of the proposed shape-memory mechanism during heating and cooling(F)

Rheological measurements showed that the storage modulus (G') remained greater than the loss modulus (G'') throughout the heating process, confirming the structural integrity of the gel. However, above 60 ℃, both moduli decreased rapidly, and a peak in the loss factor (tanδ) appeared at 62.39 ℃, corresponding to T_g. This transition reflected the change from a glassy to a highly elastic state [Fig.4(C)]. The T_g value was further corroborated by DSC analysis, which gave a transition temperature of 62.06 ℃ [Fig.4(D)], consistent with the mechanical and rheological data. At temperatures below T_g, strong hydrogen bonds restricted chain mobility, resulting in a plastic mechanical response. Above T_g, hydrogen bonds dissociated, allowing polymer chains to move freely and imparting soft, elastic behavior.

The temperature response of P(VI-*co*-MAAC-NE) hydrogel was rapid and reversible. When immersed in 70 ℃ water, the hydrogel softened quickly. Upon returning to room temperature, it rapidly regained its original stiffness. This efficient switching enabled robust shape-memory performance. A rigid strip of P(VI-*co*-MAAC-NE) was placed in hot water to dissociate hydrogen bonds, softened, and manually bent into various digital shapes. After being transferred back to ambient conditions, hydrogen bonds reformed immediately, fixing the deformed configuration [Fig.4(E) and (F)]. Notably, since the shape-memory process involved negligible volumetric change, the aggregation state of NE molecules and the resulting strong green fluorescence remained unaltered throughout the deformation and fixation steps.

3.5 Applications

Leveraging the multi-stimuli responsiveness of P(VI-*co*-MAAC-NE) hydrogel, we demonstrated its potential for advanced information encryption and anti-counterfeiting through programmable fluorescence and shape changes mediated by reversible hydrogen-bond interactions. As illustrated in Fig.5, a pristine hydrogel strip was first heated in hot water to dissociate hydrogen bonds, softened, and physically folded into the digit "6". Cooling to room temperature reformed the hydrogen bonds, permanently fixing the shape under green emission, thus writing the first message. Immersing the "6"-shaped gel in DMSO disrupted both the hydrogen-bonding network and NE aggregation, causing the gel to swell and become soft and non-emissive, thereby erasing the message. Dialyzing the organogel back into water restored the original compact structure, along with the mechanical strength and green fluorescence.

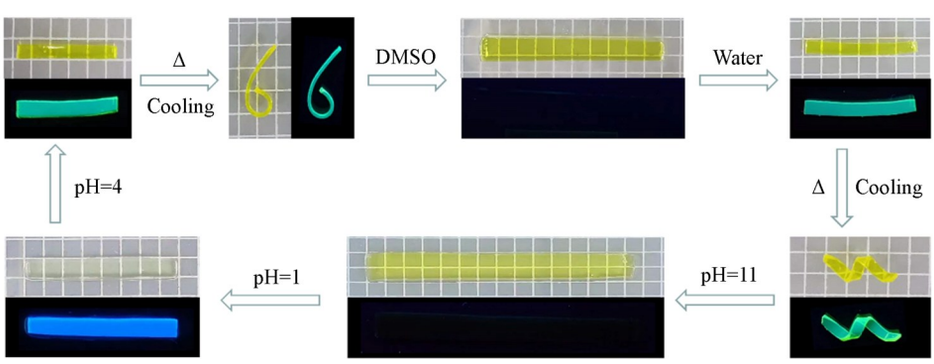

Fig. 5 Programmable information encryption and erasure *via* multi-stimuli-responsive shape and fluorescence switching

In a second writing step, the same strip was reheated and twisted into a helical shape, which was again fixed upon cooling. This new configuration could be erased by placing the helix in an alkaline solution (pH=11), where deprotonation of carboxyl groups broke the hydrogen bonds and induced strong electrostatic repulsion. This led to extreme swelling and dispersion of NE aggregates, resulting in fluorescence quenching. Subsequent transfer into an acidic solution (pH=1) protonated the imidazole groups and the *N*,*N*-diethylaniline units of NE, disrupting the ICT process. The gel remained swollen and soft, but its emission turned to intense blue. Finally, adjusting the pH to 4 allowed reformation of hydrogen bonds between

imidazole and carboxylate groups, restoring the compact gel structure. The concurrent recovery of the unprotonated diethylaniline group restored the D-π-A structure and ICT behavior, switching the emission back to strong green, while the restricted molecular motion within the contracted network enhanced NE aggregation, fully recovering the fluorescence intensity.

4 Conclusions

Based on the comprehensive investigations presented in this work, we have successfully developed a multifunctional fluorescent hydrogel, P(VI-*co*-MAAC-NE), *via* the covalent integration of an AIEgen (NE) into a dynamic hydrogen-bonding network constituted by imidazole and carboxylic acid moieties. This rational design enables orthogonal and reversible modulation of fluorescence emission, mechanical strength, and shape-memory behavior in response to multiple external stimuli, including organic solvents, pH variations, and temperature fluctuations. The robust hydrogen-bonding network not only endows the hydrogel with exceptional mechanical robustness, but also effectively restricts the intramolecular motion of the AIEgen NE, thereby eliciting intense green fluorescence in the aggregated state. More importantly, the dynamic and reversible nature of these hydrogen bonds enables the system to exhibit distinct, programmable responses: organic solvent-induced swelling coupled with fluorescence quenching; acid-triggered blue-shifted emission; alkali-driven expansion and fluorescence quenching; and thermally activated shape memory with excellent recyclability. By harnessing these multi-stimuli-responsive characteristics, we demonstrate the great potential of the P(VI-*co*-MAAC-NE) hydrogel for advanced information encryption and anti-counterfeiting applications, wherein visual and geometric outputs can be reversibly manipulated in a highly coordinated manner. This work not only provides a practical material platform for sensing and information storage, but also offers new insights into the design of intelligent soft matter systems that synergistically integrate AIE characteristics with dynamically regulated supramolecular network structures.

The supporting information of this paper see http://www.cjcu.jlu.edu.cn/CN/10.7503/cjcu20250381.

References

[1] Merindol R., Delechiave G., Heinen L., Catalani L. H., Walther A., *Nat. Commun.*, **2019**, *10*, 528
[2] Zhu Q. D., van Vliet K. V., Holten-Andersen N., Miserez A., *Adv. Funct. Mater.*, **2019**, *29*, 1808191
[3] Kang X. H., Zhang L. P., Jia W., Yang L., Jiang C. L., *Anal. Chem.*, **2024**, *96*, 20568—20577
[4] Zhang L. B., Jean S. R., Ahmed S., Aldridge P. M., Li X. Y., Fan F. J., Sargent E. H., Kelley S. O., *Nat. Commun.*, **2017**, *8*, 381
[5] Wei S. X., Li Z., Lu W., Liu H., Zhang J. W., Chen T., Tang B. Z., *Angew. Chem. Int. Ed.*, **2021**, *60*, 8608—8624
[6] Ghorai S., Dasgupta S., Mukherjee A., Barui A., Roymahapatra G., Ganguly J., *ACS Appl. Bio Mater.*, **2024**, *7*, 5640—5650
[7] Wu S. S., Shi H. H., Lu W., Wei S. X., Shang H., Liu H., Si M. Q., Le X. X., Yin G. Q., Theato P., Chen T., *Angew. Chem. Int. Ed.*, **2021**, *60*, 21890—21898
[8] Zhang Y. D. Y., Zheng T. T., Jiang S. M., *Dyes Pigments*, **2023**, *220*, 111658
[9] Lou K., Hu Z. Q., Zhang H. W., Li Q. Y., Ji X. F., *Adv. Funct. Mater.*, **2022**, *32*, 2113274
[10] Sun Y., Le X. X., Zhou S. Y., Chen T., *Adv. Mater.*, **2022**, *34*, 2201262
[11] Luo Q. Y., Jiang J., Dai J. G., Li D. X., Ren H. Z., Fu H. C., Tang A. H., Xu Y. T., Zeng B. R., Luo W. A., Dai L. Z., *Int. J. Biol. Macromol.*, **2025**, *320*, 145897
[12] Luo Q. Y., Yuan H. M., Zhang M., Jiang P., Liu M., Xu D., Guo X., Wu Y. Q., *J. Hazard. Mater.*, **2021**, *401*, 123432
[13] Shi D. W., Ji D. H., Li X., Guan Z. C., Li M. H., Bae J., *ACS Nano*, **2025**, *19*, 19578—19589
[14] Niklaus L., Tansaz S., Dakhil H., Weber K. T., Pröschel M., Lang M., Kostrzewa M., Coto P. B., Detsch R., Sonnewald U., Wierschem A., Boccaccini A. R., Costa R. D., *Adv. Funct. Mater.*, **2017**, *27*, 1601792
[15] Chen H., Yang F. Y., Chen Q., Zheng J., *Adv. Mater.*, **2017**, *29*, 1606900
[16] Ji X. F., Wu R. T., Long L. L., Ke X. S., Guo C. X., Ghang Y. J., Lynch V. M., Huang F. H., Sessler J. L., *Adv. Mater.*, **2018**, *30*, 1705480
[17] Zhu Q. D., Zhang L. H., Van Vliet K., Miserez A., Holten-Andersen N., *ACS Appl. Mater. Interfaces*, **2018**, *10*, 10409—10418

[18] Bhattacharya S., Phatake R. S., Barnea S. N., Zerby N., Zhu J. J., Shikler R., Lemcoff N. G., Jelinek R., *ACS Nano*, **2019**, *13*, 1433—1442
[19] Saigusa H., Lim E. C., *Acc. Chem. Res.*, **1996**, *29*, 171—178
[20] Li J., Wang J. X., Li H. X., Song N., Tang B. Z., Wang D., *Chem. Soc. Rev.*, **2020**, *49*, 1144—1172
[21] Luo J. D., Xie Z. L., Lam J. W. Y., Cheng L., Chen H. Y., Qiu C. F., Kwok H. S., Zhan X. W., Liu Y. Q., Zhu D. B., Tang B. Z., *Chem. Commun.*, **2001**, (18), 1740—1741
[22] Hu R. R., Leung N. L. C., Tang B. Z., *Chem. Soc. Rev.*, **2014**, *43*, 4494—4562
[23] Zhang R. B., Tian X. Q., Zuo M. Z., Zhang T., Pangannaya S., Hu X. Y., *Adv. Sci.*, **2025**, *12*, 2504993
[24] He Z. K., Ke C. Q., Tang B. Z., *ACS Omega*, **2018**, *3*, 3267—3277
[25] Zhao Z., Zhang H. K., Lam J. W. Y., Tang B. Z., *Angew. Chem. Int. Ed.*, **2020**, *59*, 9888—9907
[26] Yang C. X., Xiao H. X., Tang L., Luo Z. C., Luo Y., Zhou N. B., Liang E. X., Wang G. X., Tang J. X., *Mater. Horiz.*, **2023**, *10*, 2496—2505
[27] Wang Q., Kang M. M., Wang D., Tang B. Z., *Coord. Chem. Rev.*, **2026**, *548*, 217227
[28] Jin Q., Zeng R. P., Chen X. H., You Z., Bai W. B., Yang H. P., *Dyes Pigments*, **2025**, *239*, 112797
[29] Guo H. L., Zhu C. J., Yuan Z. H., Huang G., Liang H. S., Xiong C. X., Feng Z. Y., Wei Q., Meng G. Z., *ACS Appl. Mater. Interfaces*, **2023**, *15*, 8530—8536
[30] Yuan Z. H., Zhu C. J., Huang G., Lei B., Wu M. M., Feng Z. Y., Yang Z. Y., Wei Q., Meng G. Z., Guo H. L., *ACS Appl. Polym. Mater.*, **2024**, *6*, 10467—10477
[31] Vazquez-Perez F. J., Gila-Vilchez C., Duran J. D. G., Zubarev A., Alvarez de Cienfuegos L., Rodriguez-Arco L., Lopez-Lopez M. T., *Polymer*, **2021**, *230*, 124093
[32] Li Z., Ji X. F., Xie H. L., Tang B. Z., *Adv. Mater.*, **2021**, *33*, 2100021
[33] Lu W., Wei S. X., Shi H. H., Le X. X., Yin G. Q., Chen T., *Aggregate*, **2021**, *2*, e37
[34] Li Z., Liu P. C., Ji X. F., Gong J. Y., Hu Y. B., Wu W. J., Wang X. N., Peng H. Q., Kwok R. T. K., Lam J. W. Y., Lu J., Tang B. Z., *Adv. Mater.*, **2020**, *32*, 1906493
[35] Zhang X. N., Wang Y. J., Sun S., Hou L., Wu P., Wu Z. L., Zheng Q., *Macromolecules*, **2018**, *51*, 8136—8146
[36] Jiao C., Zhang J. N., Liu T. Q., Peng X., Wang H. L., *ACS Appl. Mater. Interfaces*, **2020**, *12*, 44205—44214
[37] An B. K., Gierschner J., Park S. Y., *Acc. Chem. Res.*, **2011**, *44*, 1570—1579
[38] Zhu C. N., Bai T. W., Wang H., Ling J., Huang F. H., Hong W., Zheng Q., Wu Z. L., *Adv. Mater.*, **2021**, *33*, 2102023
[39] Ding H. Y., Zhang X. N., Zheng S. Y., Song Y. H., Wu Z. L., Zheng Q., *Polymer*, **2017**, *131*, 95—103
[40] Palakollu V., Kanvah S., *New J. Chem.*, **2014**, *38*, 5736—5746
[41] Wang X. X., Ding Z. Y., Ma Y., Zhang Y. P., Shang H. X., Jiang S. M., *Soft Matter*, **2019**, *15*, 1658—1665
[42] Xu M. D., Hua L. Q., Gong L. H., Lu J. L., Wang J. H., Zhao C. Z., *Sci. China Chem.*, **2021**, *64*, 1770—1777
[43] Yang C. X., Su F., Xu Y. X., Ma Y., Tang L., Zhou N. B., Liang E. X., Wang G. X., Tang J. X., *ACS Macro Lett.*, **2022**, *11*, 347—353
[44] Dai C. F., Zhang X. N., Du C., Frank A., Schmidt H. W., Zheng Q., Wu Z. L., *ACS Appl. Mater. Interfaces*, **2020**, *12*, 53376—53384
[45] Wang Y. J., Zhang X. N., Song Y. H., Zhao Y. P., Chen L., Su F. M., Li L. B., Wu Z. L., Zheng Q., *Chem. Mater.*, **2019**, *31*, 1430—1440

(Ed.: Y, K, M)